

NH₃ spatio-temporal variability over Paris, Mexico and Toronto and its link to PM_{2.5} during pollution events

Camille Viatte¹, Rimal Abeed¹, Shoma Yamanouchi^{2,3}, William Porter⁴, Sarah Safieddine¹, Martin Van Damme^{5,6}, Lieven Clarisse⁴, Beatriz Herrera^{2,7}, Michel Grutter⁷, Pierre-Francois Coheur⁴, Kimberly Strong², and Cathy Clerbaux^{1,5}.

¹LATMOS/IPSL, Sorbonne Université, UVSQ, CNRS, 75252 Paris Cedex 05, France;

²Department of Physics, University of Toronto, Toronto, ON M5S 1A7, Canada;

³Department of Civil and Mineral Engineering, University of Toronto, Toronto ON M5S 1A4, Canada;

⁴Department of Environmental Sciences, University of California, Riverside, CA 92521, USA;

⁵Université libre de Bruxelles (ULB), Spectroscopy, Quantum Chemistry and Atmospheric Remote Sensing (SQUARES), Brussels 1050, Belgium;

⁶BIRA-IASB - Belgian Institute for Space Aeronomy, Brussels 1180, Belgium;

⁷Instituto de Ciencias de la Atmósfera y Cambio Climático, Universidad Nacional Autónoma de México, Mexico City, 04510, Mexico;

Correspondence: Camille Viatte (camille.viatte@latmos.ipsl.fr)

Abstract

Megacities can experience high levels of fine particulate matter ($\text{PM}_{2.5}$) pollution linked to ammonia (NH_3) mainly emitted from agricultural activities. Here, we investigate such pollution in the cities of Paris, Mexico and Toronto, each of which have distinct emission sources, agricultural regulations, and topography. Ten years of measurements from the Infrared Atmospheric Sounding Interferometer (IASI) are used to assess the spatio-temporal NH_3 variability over and around the three cities.

In Europe and North America, we determine that temperature is associated with the increase in NH_3 atmospheric concentrations with coefficient of determination (r^2) of 0.8 over agricultural areas. The variety of the NH_3 sources (industry and agricultural) and the weaker temperature seasonal cycle in southern North America induce a lower correlation factor ($r^2 = 0.5$). The three regions are subject to long range transport of NH_3 , as shown using HYSPLIT cluster back-trajectories. The highest NH_3 concentrations measured at the city scales are associated with air masses coming from the surrounding and north-northeast regions of Paris, the south-southwest areas of Toronto, and the southeast/southwest zones of Mexico City.

Using NH_3 and $\text{PM}_{2.5}$ measurements derived from IASI and surface observations from 2008 to 2017, annually frequent pollution events are identified in the three cities. Wind roses reveal statistical patterns during these pollution events with dominant northeast-southwest directions in Paris and Mexico City, and the transboundary transport of pollutants from the United-States in Toronto. To check how well chemistry transport models perform during pollution events, we evaluate simulations made using the GEOS-Chem model for March 2011. In these simulations we find that NH_3 concentrations are overall underestimated, though day-to-day variability is well represented. $\text{PM}_{2.5}$ is generally underestimated over Paris and Mexico, but overestimated over Toronto.

1. Introduction

Paris, Toronto, and Mexico City are cities with over 2 million inhabitants. When their larger metropolitan regions are included, their populations are 10.5 million for Paris (the most populous area in the European Union), 6.5 million for Toronto (the fourth most populous city in North America) and 9.2 million for Mexico City (most populous city in North America). These cities typically experience strong particulate matter (PM) pollution episodes. Exposure to such particles is harmful to humans and can lead to cardiovascular and respiratory diseases [Murray et al., 2020].

A large proportion of the particles' composition is ammonium sulfate and nitrate, which are formed from ammonia (NH_3) [Behera et al., 2013] released in the atmosphere from e.g., fertilizer spreading practices and both transported to cities, reducing the quality of urban air [Pope et al., 2009]. The agricultural sector represents 94%, 90%, and 94% of total NH_3 emissions in France [CITEPA, 2018], Canada [ECCC, 2017] and Mexico [INECC and SEMARNAT, 2018], respectively. NH_3 is the most poorly understood precursor of $\text{PM}_{2.5}$ (PM with a diameter less than $2.5 \mu\text{m}$), primarily because measurements are difficult [von Bobritzki et al., 2010], sparse, and due to low ambient NH_3 concentrations and episodic emissions. Worldwide, only five countries (United States, China, Netherlands, United Kingdom, and Canada) have included routine measurements of NH_3 concentrations in their air quality monitoring networks [Nair and Yu, 2020].

NH_3 emissions are associated with very high uncertainties in all inventories (186% to 294% uncertainties in EDGAR [McDuffie et al., 2020; Van Damme et al., 2018]) due to uncertainties in the reporting of agricultural statistics and emission factors that depend on individual agricultural practices, biological processes, and environmental conditions [Paulot et al., 2014], as well as political disturbances and land-use change [Abeed et al., 2021]. The evaporation of NH_3 in the atmosphere, as well as its transformation into particulate matter, is highly dependent on the thermodynamic conditions of the atmosphere [Sutton et al., 2013]. All these parameters account for the complexity of reproducing NH_3 concentrations in atmospheric models, predicting the associated $\text{PM}_{2.5}$ pollution, and, ultimately, implementing relevant regulations to reduce its emissions.

Given the crucial role that NH_3 plays in environmental and public health problems, reducing its emissions will therefore be a major challenge. However, NH_3 concentrations are increasing in many countries: France, Canada and Mexico reported increases of $24 \pm 11\%$, $16.4 \pm 8.6\%$, and $8.4 \pm 5.2\%$ between 2008 and 2018 respectively [Van Damme et al., 2021]. These trends are likely explained by increasing emissions, partly due to increased temperature (Europe) and biomass burning (Canada). However, decreasing concentrations of nitrogen and sulfur oxides e.g. in Europe and China also increase the ammonia atmospheric lifetime and plays a role in the reported upward trends.

In Paris, $\text{PM}_{2.5}$ are composed of organic matter (38–47 %), nitrate (17–22 %), non-sea-salt sulfate (13–16 %), ammonium (10–12 %), and to a minor extend with elemental carbon, mineral dust (2–5 %) and sea salt [Bressi et al., 2013]. In springtime, it has been shown that NH_3 plays a significant role in $\text{PM}_{2.5}$ pollution episodes [Viatte et al., 2021] but long-term observations are needed to properly evaluate the impact of NH_3 to $\text{PM}_{2.5}$ formation.

In Toronto, secondary nitrate formed from nitric acids (NO_x) and NH_3 account for 36% of the $\text{PM}_{2.5}$ sources [Lee et al., 2003] and ammonium nitrate and sulfate accounted for 20-30% of annual $\text{PM}_{2.5}$ mass over the 14-year period between 2006 and 2014 [Jeong et al., 2020]. There is a need for a higher number of surface observations to evaluate the NH_3 - $\text{PM}_{2.5}$ relationship and its evolution over time [Larios et al., 2018].

In Mexico, PM_{2.5} concentrations often exceed the national standard of 41 µg/m³ for the 24-hour mean [NOM-025-SSA1-2021, 2021]. Secondary inorganic aerosols account for 30% of the chemical composition of PM_{2.5}, which are dominated by ammonium sulfate with an average of 14% [Vega et al., 2010]. A better understanding of the particulate pollutants processes in Mexico is still needed [Ojeda-Castillo et al., 2019].

To assess the role of NH₃ in the formation of particulate matter, the AmmonAQ (Ammonia air quality) project was designed to quantify NH₃ spatio-temporal variabilities in regional domains around these three cities. The main objective of this project is to determine the impact of intensive agricultural practices on NH₃ and urban air quality, with a focus on Paris, Toronto and Mexico as benchmark case studies. A schematic representation of the AmmonAQ project and the domains of study are shown in Figure 1. The so-called “Europe”, “North America”, and “southern North America” domains represent the extended area with NH₃ sources that can impact on the Paris, Toronto, and Mexico cities air composition. The three cities are investigated with the use of different datasets: satellite measurements and model simulation data, and surface measurements when available (see section 2).

These cities have been chosen as the focus of this study because of the availability of NH₃ and PM_{2.5} measurements. These three cities differ in terms of:

1. The regulation of NH₃ emissions: French policies aim to reduce NH₃ emissions by 13% in 2030 relative to 2005 [CEIP, 2016] following EU ratification of the Gothenburg Protocol in 2017, whereas in Canada and Mexico there are no federal regulations for NH₃ emissions yet [Bittman et al., 2017];
2. Agricultural practices affecting NH₃ emissions differ in each region as farmers depend on meteorological conditions for fertilizer use;
3. Meteorological/climate conditions are very different in each of the regions: drier winter and wetter summer in Toronto compared to Paris, and weak winds and strong temperature inversions in Mexico-city. This influences the NH₃ lifetime and chemistry leading to the formation of PM_{2.5};
4. Topography: Toronto is adjacent to Lake Ontario, Paris is inland, and Mexico-city is a basin surrounded by mountains. This will impact the trajectories of air masses.

2. Methodology

2.1. NH₃ observations derived from IASI

The Infrared Atmospheric Sounding Interferometer (IASI) was launched onboard the Metop-A/B/C satellites in 2006, 2012, and 2018, respectively [Clerbaux et al., 2009]. IASI provides twice daily total column measurements of NH₃ globally at 9:30 and 21:30 local solar time. With its polar orbit and a swath of 2400 km, IASI pixel size is 12 km in diameter at nadir. In this work, we use version 3 of the ANNI-NH₃ product [Van Damme et al., 2021; Guo et al., 2021] from IASI Metop-A/B morning overpasses over the period 2008 to 2017 gridded a spatial resolution of 0.25° x 0.25°. The detection limit depends both on the atmospheric state (mainly thermal contrast and NH₃ abundance) and the instrument characteristics. For IASI, the minimum detection limit is found to be 4-6x10¹⁵ molecules/cm² [Clarisse et al., 2010].

2.2. PM_{2.5} dataset derived from surface network measurements

To study local scale PM_{2.5} pollution events in the Paris, Toronto, and Mexico cities, PM_{2.5} observations of surface concentrations from 2008 to 2017 are used.

For Paris, we use hourly observations of PM_{2.5} concentrations derived from fourteen stations of the Airparif network (<https://data-airparif-asso.opendata.arcgis.com/>). For Toronto, we analyze hourly PM_{2.5} observations derived from eleven stations supported by the Ministry of the Environment, Conservation and Parks of Ontario (<http://www.airqualityontario.com/>). For Mexico, PM_{2.5} concentrations are derived from 27 stations of the Red Automática de Monitoreo Atmosférico (RAMA, <http://www.aire.cdmx.gob.mx/default.php?opc=%27aKBh%27>) network.

All these stations are located within a circle of 50-km radius around the city centers of Paris, Toronto, and Mexico City.

2.3. NH₃ and PM_{2.5} from the GEOS-Chem model

We generate model outputs for March of 2011 because all three cities experienced both separate and combined PM_{2.5} and NH₃ pollution events during this period. We use version 12.7.2 of the GEOS-Chem chemical transport model [Bey et al., 2001] driven by the MERRA-2 reanalysis product, including nested domains over Europe and North America at a 0.5° × 0.625° horizontal resolution from which we extract modeled surface values for each city. Boundary conditions for these two nested domains are created using a global simulation for the same month at 2° × 2.5° resolution. Output for the analyzed month of March includes monthly means, as well as hourly means for selected diagnostics, and is preceded by two months of discarded model spinup time for the global simulation, and one month for each nested run. Anthropogenic emissions are taken primarily from the global Community Emissions Data System (CEDS) inventory [Hoesly et al., 2018], with regional emissions from the 2011 National Emissions Inventory produced by the US EPA (NEI2011) used to override global values over the United States. Biogenic non-agricultural ammonia, as well as ocean ammonia sources, are taken from the Global Emission Inventories Activities database (GEIA, [Bouwman et al., 1997]). Open fire emissions are generated using the GFED 4.1s inventory [Randerson et al., 2017]. Sulfate-nitrate-ammonium aerosol processes are calculated using version 2.2 of the ISORROPIA thermodynamic module [Fountoukis and Nenes, 2007]. Black carbon is handled as described in Wang et al. (2014), while secondary organic aerosol is produced using the simplified irreversible scheme described in Pai et al., (2020).

2.4. Back-trajectories analysis from the HYSPLIT model

To determine the effect of long-range transport affecting the local air quality of the three cities, we use the Hybrid Single-Particle Lagrangian Integrated Trajectory model (HYSPLIT, [Stein et al., 2015]). Note that unlike the GEOS-Chem model, HYSPLIT does not include atmospheric chemistry. For the runs, meteorological data are from the National Centers for Environmental Prediction (NCEP) / National Center for Atmospheric Research (NCAR) reanalysis at 2.5-degree global latitude-longitude projection. Note that results using a finer meteorological dataset (GDAS at 1° resolution) show no significant differences. First, we run daily 24-hour back-trajectories ending in the city-centers at the overpass time of the IASI instrument covering the period 2008 to 2017. Then, for each day we calculate the mean of NH₃ total columns derived from IASI observations in a 50-km radius circle around the cities associated with each back-trajectory. Finally, all back-trajectories that are near to each other are merged in clusters and associated with the corresponding local-scale IASI NH₃ concentrations.

2.5. ERA-5 meteorological data

The meteorological variables used in this study are extracted from the hourly ECMWF's reanalysis (ERA5, [Hersbach et al., 2020]). ERA5 data are at 0.25° × 0.25° resolution (native horizontal resolution of ERA5 is ~31km) and are interpolated in time and space to the IASI observation. The meteorological parameters considered here are the skin temperature (T_{skin}, which is the physical temperature of the Earth's surface), total precipitation (in meter of water equivalent - accumulated liquid and frozen

water, comprising rain and snow -) and relative humidity up to 2 meters above the surface calculated from dew and air temperature at 2m from ERA5.

3. Results

3.1. NH₃ source regions identification and spatio-temporal variability over the Europe, North America, and southern North America domains

Using 10-years of IASI observations, the main source regions of NH₃ in the 3 domains of study are identified (Figure 2) and listed in Table 1. We identify 10, 9, and 19 NH₃ source regions over the Europe, North America, and southern North America regions, respectively. All of the sources over the Europe, North America domains are mostly related to agricultural practices (farming and spreading practices). This is in agreement with previous calculation of worldwide nitrogen inputs from fertilizer and manure [Potter et al., 2010]. Around southern North America, three sources are related to fertilizer or soda ash industries (listed with C, G, O in Figure 2 and Table 1, [Van Damme et al., 2018]), the rest is agricultural.

Spatio-temporal variabilities of NH₃ in the atmosphere in the three regions (Figure 2) are not expected to be similar: NH₃ emissions from industries in the region of southern North America are released all year long, whereas NH₃ emissions from agricultural practices (which are dominant over Europe and North America), depend on various surface and meteorological conditions. In order to investigate this, NH₃ concentrations using 10-years of IASI observations are assessed against atmospheric temperature and precipitation derived from the ERA5 reanalysis over the three domains in Figure 3. It shows the seasonal evolution of NH₃ from IASI over the three regions (left panel), along with the seasonal evolution of temperature and precipitation (right panel).

For Europe and North America, NH₃ total columns are the highest in spring and summer. In fact, NH₃ concentrations over Europe exhibit two seasonal maxima in March/April and July/August (supplementary material, Figure S1) and in North America the maxima are in May and September (Figure S2). This is consistent with agricultural practices (i.e. fertilizer application) and higher air temperature favoring NH₃ volatilization in the atmosphere.

The right panel of Figure 3 shows how temperature (red lines) and precipitation (blue bars) seasonally evolve over the three regions. In winter, atmospheric temperatures are below 5 °C in Europe and North America, and IASI observations reveal almost no NH₃ hot spots (left panel, Figure 3). This can be due to the lack of NH₃ abundance, lower volatilization in this temperature range, no agricultural emissions in winter and/or the reduced sensitivity of the IASI NH₃ retrievals in winter [Van Damme et al., 2017]. The high value over Canada and the Arctic in winter can be associated with high uncertainties in the NH₃ retrievals due to low thermal contrast.

In southern North America, NH₃ seasonal variations are less pronounced than in the other two regions. Figure 3 shows that the NH₃ concentrations over several sources, such as Torreon and San Juan de Los Lagos (boxes B and F in Figure 2 right panel) are high during all seasons, which could be associated with the weak seasonal cycle of temperature in this region closer to the equator.

In spring, seasonal precipitations are the lowest for the three regions. This is reflected in high NH₃ concentrations on the left panel. Over Europe and North America, this can be related to agricultural spreading practices period and higher atmospheric temperature favoring NH₃ volatilization. In southern North America, NH₃ concentrations observed by IASI are the highest in spring when atmospheric temperatures are high and precipitations rates are low. In addition, biomass burning, that are often encountered during this period could explain higher atmospheric NH₃ concentrations in

spring. NH_3 reach maximum values in April/May (Figure S3) just before the start of the rain season, potentially reducing observed NH_3 concentrations due to the wet deposition of atmospheric gaseous ammonia [Asman et al., 1998].

Since in Europe and North America NH_3 sources are mostly agriculture-related (with small contributions from industries), the temperature/ NH_3 relationship is expected to be relatively easy to interpret: when the land surface temperature increases, volatilization of ammonia from the fertilized/manured soil is favored, and atmospheric ammonia increases. The corresponding determination factors r^2 for this relationship in Europe and North America are 0.85 and 0.80 respectively (polynomial fit of second order). This is not the case in southern North America, in which some of the ammonia sources are also industrial and they contribute greatly to the atmospheric NH_3 , the concentrations of ammonia are therefore not directly temperature dependent, as we can see on the right upper panel in Figure S4 ($r^2 = 0.46$). There is nonetheless a relationship in southern North America that is due to the fact that we have constant high ammonia sources and temperatures (Figure 3). In fact, the relationships between NH_3 and temperature on one hand, and precipitation/relative humidity on the other hand, are not linear; this has been equally shown in a previous study [Sutton et al., 2013].

To further investigate the temperature/ NH_3 relationship, we show in Figure 4 the evolution of NH_3 with respect to land surface temperature over different sub-regions of the Europe domain (listed in Table 1). Similar Figures for the North America and southern North America domains are shown in the supplement information (Figure S5 and S6). We observe a peak of NH_3 followed by a local maximum plateau between 10 and 25°C approximately in all of the regions of the Europe domain (Figure 4). In fact, the NH_3 detected in this range of temperature can indicate the fertilizer application period, since most of them (up to 80%) were detected during the spring and fall seasons. For instance, over the Po valley (region F in Table 1, Figure 4), 36% of the NH_3 detected in the bins 10 – 25°C correspond to the spring season, whereas 35% correspond to the fall season (not shown here). In Celina-Coldwater (region G in Table 1), 82% of the NH_3 detected between 10 and 25°C correspond to the spring and the fall seasons, the percentage is split equally (Figure S5).

We choose to show the sub regions in the vicinity of the Europe domain, since they are mostly agricultural sources. The “bumps” corresponding to the fertilizer application are very clear in all of the sub-regions. This bump was detected to a lower extent for agricultural regions affecting North America (supplementary material Figure S5). Over the agricultural regions in the southern North America domain, the bumps are clear in the regions A to D (Figure S6, a). When the seasonal temperatures do not fluctuate during the fertilizer application, any increase in atmospheric NH_3 is due to the sudden addition of nitrogen fertilizers to the soil. In southern North America, the regions E to M show that the highest NH_3 concentrations were observed as the temperature increased during the growing seasons (Figure S6). A possible explanation to the resemblance among the regions A to D is that they share similar climate properties (Steppe and Desert) unlike the rest of the sub-regions in the same domain (tropical/subtropical). Since the temperatures in the Europe and southern North America domains are higher (Figure 3, right panels) in spring and fall seasons (fertilizer application period) than those in North America, this bump is clearer in the latter. The bumps seen for the Europe regional domain are clearer than those of southern North America, possibly related to the fact that in autumn in Europe precipitation is lower than those in southern North America, leading to lower NH_3 loss through wet deposition.

3.2. NH₃ budget over the cities of Paris, Toronto, and Mexico

Temperature, relative humidity, and precipitation are not the only factors affecting the NH₃ concentrations. In order to analyze the impact of long-range transport on NH₃ concentrations measured over the cities (and not domains) of Paris, Toronto, and Mexico, HYSPLIT back-trajectories have been used. For each day of IASI NH₃ observations made in a 50-km radius circle from the city-center, a 24-hours back-trajectory has been performed from 2008 to 2017. There are between 3643 and 4008 back-trajectories for Paris, Toronto, and Mexico cities. Then, a seven-cluster analysis has been applied to these datasets and NH₃ mean concentrations measured inside the cities by IASI have been allocated to the different mean cluster trajectories according to the corresponding back-trajectories. Details about this analysis are described in the supplementary material Figure S7. The result is shown in Figure 5.

For Paris, 1/4 of all back-trajectories (875) that are associated with the highest NH₃ concentrations, i.e. 4.71×10^{15} molecules/cm² on average, are originating from the surrounding south regions (black line, Figure 5). Clusters 2 and 3 are also associated with high NH₃ concentrations and are coming from the north-northeast. This is consistent with previous analyses using HYSPLIT [Viatte et al., 2020] and FLEXPART models [Viatte et al., 2021]. As expected, the back-trajectories coming from the ocean are related with almost no NH₃ concentrations (light and dark blue lines, left panel).

Over Toronto, the highest NH₃ concentrations (24% and 14%) measured in the city are allocated to long-range transport located south-southwest (black and purple lines, middle panel) coming from the United-States where most of the feedlots are. 9 to 17% of NH₃ concentrations are coming from the west and the east of Toronto (cluster 3, 4, and 5) where atmospheric NH₃ have increased in the last decade (Boxes A and B in Figure 2, [Yao and Zhang, 2019]). The 2 back-trajectory clusters that are related to low NH₃ concentrations are coming from the north (light and dark blue lines) where no NH₃ sources have been identified.

In the southern North America domain, back-trajectories are coming from relatively close regions since orographic conditions around Mexico-city limit long-range transport. In this city, the highest NH₃ concentrations are associated with air masses coming from the southwest (11%, black line, 22%, purple line, right panel) and southeast (27%, red line). Air parcels coming from the north are associated with relatively low NH₃ concentrations measured in Mexico City.

3.3. Pollution events over Paris, Toronto, and Mexico cities from 2008 to 2017

After assessing the NH₃ distribution under average climate conditions, we focus now on pollution events occurring at the three cities. These are identified by applying the Fourier series of order 3 [Yamanouchi et al., 2021; Herrera et al., 2022] on the surface PM_{2.5} and satellite NH₃ observations at cities scale (i.e. 50-km radius circle from city-centers). The Fourier fit accounts for the “natural” variability (seasonality) in the time-series, and helps identify pollution events that are 2 standard deviations above this natural variability. It is a robust method commonly used to quantify trends and identify enhancements in long-term timeseries [Zellweger et al., 2009]. Pollution events occurrence per city per year (a) and per season (b) are shown in Figure 6.

The figure shows that NH₃ pollution episodes are found to be annually frequent at the three cities. In Toronto and Mexico cities, PM_{2.5} pollution events are encountered annually (with higher number in Mexico) whereas no events are detected in 2009, 2015, and 2017 in Paris.

Numbers of identified days of PM_{2.5} pollution events are 88, 58, and 50 in Mexico City, Toronto, and Paris, respectively. For NH₃ pollution events, they occur more in Toronto than in Mexico City and Paris,

with number of days of 94, 73, and 56, respectively. Common days of high NH_3 and $\text{PM}_{2.5}$ concentrations are found in all three cities, especially in spring (Figure 6b), coinciding with the high seasonal NH_3 concentrations shown in Figure 3.

To further investigate the impact of transport on pollution events occurring at the three cities, we have analyzed the wind fields patterns for different cases: i) for the whole dataset (i.e. ensemble 2008-2017), ii) for days of NH_3 and $\text{PM}_{2.5}$ pollution events occurred separately, and iii) for days when both high concentrations are observed. Figure 7 shows wind roses computed for the ensemble and these different types of pollution events (i.e. $\text{PM}_{2.5}$, NH_3 and both occurring during the same day). The radial distance in the wind roses indicates the frequency of the wind direction occurrence. In general, wind speed is lower at Mexico City (max 3 m s^{-1}) compared to Toronto and Paris (up to 10 m s^{-1}) because of the mountainous topography that blocks and slows air masses exchange in Mexico.

In Paris, the ensemble wind-roses show a dominant northeast-southwest pattern. NH_3 pollution events are associated with wind coming from various directions at all wind speeds which was suggested by the HYSPLIT cluster analysis (Figure 5), whereas $\text{PM}_{2.5}$ events are present mainly under high northeast wind. When both NH_3 and $\text{PM}_{2.5}$ high concentrations are observed in Paris, the wind field can have two patterns: low wind speed coming from all direction (except from the south) or high wind speed coming from the northeast. This confirms the importance of transport of NH_3 and $\text{PM}_{2.5}$ from the northeast and could suggest the inter-conversion of $\text{PM}_{2.5}$ to NH_3 at low wind speed.

In Toronto, the ensemble show that dominant wind pattern is coming from the south. For all the pollution events (NH_3 , $\text{PM}_{2.5}$, and both) the wind is coming from the southwest, confirming the long-range transport of pollutants from the United-States.

In Mexico City, the dominant pattern (ensemble) is southwest-northeast wind fields. For days of NH_3 pollution events, wind is mainly coming from the south-southwest, and for $\text{PM}_{2.5}$, wind come from all direction with an important northeast wind pattern. Days of both pollution events are associated with wind coming from the west-southwest only.

3.4. Case study: NH_3 and $\text{PM}_{2.5}$ concentrations comparison with the GEOS-Chem model in March 2011

The occurrence of pollution events varies from year to year (Figure 6). However, in 2011, all three cities experienced $\text{PM}_{2.5}$ and NH_3 separate and combined pollution events. For this reason, GEOS-Chem model simulations were performed in March 2011 to interpret the events and evaluate the model performance.

Spatial and temporal coincidence criteria have been applied to GEOS-Chem outputs to compare with IASI morning observations, such as: model outputs between 8.30 and 11.30 AM coincident with IASI overpasses have been selected, and only collocated model outputs (at $0.5^\circ \times 0.625^\circ$ horizontal resolution) have been selected coincident with IASI observations. Averages of numbers of coincident observations are 1324, 1138, and 3000 over the Europe, North America, and southern North America domains of study during March 2011.

Figure 8 shows the one-month comparison between the two datasets. Over the regional domains, the coefficient of correlation between daily model NH_3 concentrations and IASI NH_3 observations are $R = 0.50$, $R = 0.55$, and $R = 0.33$, over Europe, North America, and southern North America, respectively, with related p -values < 0.01 . NH_3 columns derived from the GEOS-Chem model are overall underestimated with Mean Relative Difference (MRD = (model - observations) / observations) of -37%, -31%, and -2% over Europe, North America, and southern North America, respectively.

Over Europe and North America, IASI and GEOS-Chem capture some of the same pollution events (on March 12, 15, and 30 over Europe, and March 12, 13, and 18 over North America). In southern North America, the underestimation of the GEOS-Chem NH_3 columns is less pronounced (MRD is -2%) than in the other regions but the day-to-day variability is not well represented in the model.

The GEOS-Chem model NH_3 total columns are lower than those from IASI in March 2011 over specific locations in the southern North America and Europe domains (Figure 8, right panels). For the Europe region, GEOS-Chem NH_3 columns are smaller than the IASI ones over the north of France, Belgium, the Netherlands, north of Spain (in particular sources A, B, C, D, E, I, and J of Figure 2) and the United Kingdom. For the southern North America domain, GEOS-Chem NH_3 columns are smaller than the IASI ones over the west Mexican coast (sources A, D, E, J of Figure 2/Table 1), central (source F, G, H of Figure 2) and southeast (sources O and P of Figure 2) of Mexico City and over the Pacific Ocean, whereas they are higher in Guatemala (source S, R of Figure 2), and West of Mexico City.

Over the North America domain, spatial distribution of the differences between NH_3 columns derived from GEOS-Chem and IASI are less pronounced than in the Europe and southern North America domains. IASI NH_3 columns are smaller than GEOS-Chem outputs over the south of the United-States and over the Lancaster County (sources E and I of Figure 2) and higher over Indiana in the United States.

At the city scales of Paris and Mexico City, the daily model NH_3 columns are in relatively good agreements with IASI observations within a 50-km radius circle from the city-centers (not shown here), since the coefficient of correlation are $R = 0.42$ and $R = 0.52$, respectively. Similar to the regional domains, GEOS-Chem NH_3 columns are relatively underestimated at the city scales of Paris and Mexico City, with a MRD of -108% and -28%. At the city scale of Toronto, the correlation between the NH_3 columns derived from the model and observed by IASI is poor, with a coefficient of correlation of $R = -0.32$, and a small underestimation of the modelled NH_3 concentrations is found with a MRD of -6%.

Local comparison of $\text{PM}_{2.5}$ concentrations at the city scale (over Paris, Toronto, and Mexico) is shown in Figure 9, left panels. They show that $\text{PM}_{2.5}$ concentrations calculated by the model in March 2011 are in relatively better agreement with the surface observations with $R = 0.63$, $R = 0.43$, and $R = 0.54$ in Paris, Toronto and Mexico City. In Paris and Mexico City, $\text{PM}_{2.5}$ concentrations values derived from the observations are overall higher than the GEOS-Chem concentrations with MRD values of -13% and -20%, respectively, whereas GEOS-Chem $\text{PM}_{2.5}$ concentrations are higher than the observations in Toronto with MRD value of 519%.

The right panels of Figure 9 show the chemical composition of the $\text{PM}_{2.5}$ from GEOS-Chem. These inform us about the different pollution sources. Organic matter sources are splitted equally between the primary emissions and the oxidation of volatile organic compounds [Day et al., 2015]. SNA (sum of sulfate, nitrate, and ammonium) sources originate in chemical transformation of gaseous precursors in the atmosphere, whereas black carbon comes from primary emissions of industrial and traffic combustion.

According to the GEOS-Chem model, SNA dominates the $\text{PM}_{2.5}$ chemical composition mass in March 2011 over the three cities, meaning that the dominant source of $\text{PM}_{2.5}$ mass comes from the secondary oxidation path. This partition of SNA in March 2011 from the model is higher than what have been reported based on 1-year-measurements performed in 2013: 43%, 42%, and 33% of the $\text{PM}_{2.5}$ mass composition in Paris, Toronto, and Mexico City, respectively [Cheng et al., 2016].

In Paris, the March 2011 pollution episode has been analyzed in terms of geographical origins and aerosol properties [Chazette et al., 2017] but not in terms of aerosol speciation.

Comparing the GEOS-Chem outputs used in this study with two years of observations of aerosol chemical composition in Paris (2011-2013) [Petit et al., 2015], we found that the sulfate component is slightly higher in the GEOS-Chem model than in the springtime observations (21% compared to 11%) whereas modelled organic carbon is lower than the observations (8% compared to 33%). This springtime underestimation of organics in atmospheric models has previously been reported in Paris [Sciare et al., 2010; Petit et al., 2015; Lanzafame et al., 2021] and could be associated with an underestimation of the organic matter emissions from residential contributions [Van der Gon et al., 2015]. Regarding the secondary aerosol, observations in Paris during the March 2015 pollution event show that it accounts for more than 50% of the PM concentration [Petit et al., 2017], which is in agreement with the SNA partition in our GEOS-Chem model simulation.

In Toronto, PM_{2.5} speciation is monitored by the National Air Pollution Surveillance Program (NAPS, <https://www.canada.ca/en/environment-climate-change/services/air-pollution/monitoring-networks-data/national-air-pollution-program.html>) network. Observations in March 2011 reveal that inorganic nitrate burden is overestimated by a factor 2 in the GEOS-Chem run (41% in the model compared to 20% in the observations), whereas sulfate and black carbon abundances are underestimated by a factor 2 (15 and 6% in the model compared to 27 and 12% in the observations).

In Mexico City, the organic matter represents the most abundant fraction of the aerosol, which is consistent with measurements made during several campaigns performed in the dry season of 2006 during the Megacity Initiative: Local And Global Research Observations (MILAGRO, [Molina et al., 2010]) and Aerosoles en Ciudad Universitaria (ACU) in 2015 [Salcedo et al., 2018]. Observations performed during the dry-warm season of 2019 reported that SNA correspond to 30% of the aerosol mass concentration [Retama et al., 2022], which is consistent with what has been reported before [Cheng et al., 2016] and the chemical composition modelled in our study. The organic fraction is found to be dominant in the observations [Retama et al., 2022] as suggested in the GEOS-Chem model over Mexico-City. Daily cycles appear overexaggerated in the model with maxima well represented and minima greatly underestimated. This could suggest model issues in term of atmospheric dynamics (removal/transport or planetary boundary layer dynamics) due to coarseness of grid.

4. Conclusion

The AmmonAQ project aims to determine the impact of intensive agricultural practices on urban pollution in the Paris, Toronto, and Mexico metropolitan areas. For this purpose, PM_{2.5} and NH₃ measurements from in situ instruments and satellite infrared spectrometers, and atmospheric model simulations, have been combined.

Using 10-years of IASI observations, NH₃ sources regions have been identified. All of the sources are from the agricultural sector (husbandry and fertilizer application) in the Europe and North America domains, whereas, some of them are industrial in the southern North America region. Consequently, the spatio-temporal variability of NH₃ is different, with stronger seasonal variabilities in Europe and North America. A strong correlation is found between NH₃ total columns and surface temperature (T_{skin}) for all regions, with higher correlation over agricultural regions, and when the temperature seasonal cycle is pronounced. We find that the timing of the fertilizer application can be detected through local maxima in the NH₃/T_{skin} relationship curve.

According to HYSPLIT cluster analysis, the highest NH₃ concentrations measured at the city scales are associated with air masses coming from the surrounding regions: the north-northeast of Paris, the south-southwest of Toronto, and the southeast/southwest of Mexico City. These lead to the exacerbation of the degradation of air quality in each of the three cities.

Pollution episodes are found to be annually frequent at the three cities, especially in springtime when high NH_3 and $\text{PM}_{2.5}$ are observed. In Paris and Mexico pollution is transported along the northeast-southwest line, whereas, in Toronto, the transboundary transport of pollutant from the United-States is dominant during pollution events.

The evaluation of the GEOS-Chem outputs in March 2011 reveals that NH_3 concentrations are overall underestimated by the model at the regional scale, with, however, a good representability of the day-to-day variability in Europe and North America domains. NH_3 columns derived from IASI and the GEOS-Chem model exhibit substantial spatial differences in the Europe and southern North America areas. In term of $\text{PM}_{2.5}$ concentrations at the city scales, we show that they are underestimated in Paris and Mexico, but overestimated in Toronto.

The IASI thermal infrared remote sensors have proved to be valuable to monitor pollution events over cities. The main limitations are associated with the low revisit time (at the beginning and at the end of the day), the lack of sensitivity to the surface in particular in winter, and some areas are not well covered during cloudy scenes. In the near future the next generation of instruments will have improved capabilities to sound deeper in the atmosphere [Crevoisier et al., 2014]. The IRS-MTG satellite instrument that should be launched in 2024 in geostationary orbit will offer the capacity to enhance this research over Europe thanks to better temporal (measurements every 30-45 minutes) and spatial (4 km x 4 km pixel) resolution.

Data availability

The near-real-time IASI NH_3 (ANNI NH_3 -v3) data used in this study are freely available through the Aeris database <https://iasi.aeris-data.fr/nh3-i/> (Van Damme et al., 2021) (last access: 1 April 2022). All hourly observations of $\text{PM}_{2.5}$ concentrations are available from the Airparif network (<https://data-airparif-asso.opendata.arcgis.com/>), the Ministry of the Environment, Conservation and Parks of Ontario (<http://www.airqualityontario.com/>), and the Red Automática de Monitoreo Atmosférico (RAMA, <http://www.aire.cdmx.gob.mx/default.php?opc=%27aKBh%27>) network (last access: 1 April 2022). The GEOS-Chem outputs are currently available upon request. All MATLAB/PYTHON codes used to create any of the figures and/or to create the underlying data are available on request.

Author contributions

CV, CC, SY, and KS designed the AmmonAQ project. MV and LC provided the IASI data. WP provided the GEOS-Chem outputs. CV and RA analyzed the data. CV, RA, and SS wrote the manuscript draft. BH, MG, KS, P-FC, and CC reviewed and edited the manuscript.

Competing interests

The authors declare that they have no conflict of interest.

Acknowledgments

AmmonAQ results from a joint research program between CNRS (National Center for Scientific Research of France) and the University of Toronto which funded one year of common research in 2019. Research at ULB was supported by the Belgian State Federal Office for Scientific, Technical and Cultural Affairs (Prodex HIRS) and the Air Liquide Foundation (TAPIR project). LC is Research Associate supported by the Belgian F.R.S.-FNRS. This project has received funding from the European Research Council (ERC) under the European Union's Horizon 2020 and innovation programme (grant agreement

466 No 742909, IASI-FT advanced ERC grant). The MERRA-2 data used in this study have been provided by
467 the Global Modeling and Assimilation Office (GMAO) at NASA Goddard Space Flight Center.

468 References

469 Abeed, R., Clerbaux, C., Clarisse, L., Van Damme, M., Coheur, P.-F., Safieddine, S.: A space view of
470 agricultural and industrial changes during the Syrian civil war, *Elementa: Science of the Anthropocene*,
471 9(1). doi:<https://doi.org/10.1525/elementa.2021.000041>, 2021

472 Asman, W., Sutton, M. A. and Schj rring, J. K.: Ammonia: emission, atmospheric transport and
473 deposition, *New Phytol.*, 139, 27–48, 1998.

474 Bey, I., Jacob, D. J., Yantosca, R. M., Logan, J. A., Field, B. D., Fiore, A. M., Li, Q., Liu, H. Y., Mickley, L. J.
475 and Schultz, M. G.: Global modeling of tropospheric chemistry with assimilated meteorology: Model
476 description and evaluation, *J. Geophys. Res. Atmos.*, 106(D19), 23073–23095,
477 doi:<https://doi.org/10.1029/2001JD000807>, 2001.

478 Bouwman, A. F., Lee, D. S., Asman, W. A. H., Dentener, F. J., Van Der Hoek, K. W. and Olivier, J. G. J.: A
479 global high-resolution emission inventory for ammonia, *Global Biogeochem. Cycles*, 11(4), 561–587,
480 doi:<https://doi.org/10.1029/97GB02266>, 1997.

481 Chazette, P. and Royer, P.: Springtime major pollution events by aerosol over Paris Area: From a case
482 study to a multiannual analysis, *J. Geophys. Res. Atmos.*, 122(15), 8101–8119,
483 doi:<https://doi.org/10.1002/2017JD026713>, 2017.

484 Cheng, Z., Luo, L., Wang, S., Wang, Y., Sharma, S., Shimadera, H., Wang, X., Bressi, M., de Miranda, R.
485 M., Jiang, J., Zhou, W., Fajardo, O., Yan, N. and Hao, J.: Status and characteristics of ambient PM_{2.5}
486 pollution in global megacities, *Environ. Int.*, 89–90, 212–221,
487 doi:<https://doi.org/10.1016/j.envint.2016.02.003>, 2016.

488 Clarisse, L., Shephard, M. W., Dentener, F., Hurtmans, D., Cady-Pereira, K., Karagulian, F., Van Damme,
489 M., Clerbaux, C., and Coheur, P.-F.: Satellite monitoring of ammonia: A case study of the San Joaquin
490 Valley, *J. Geophys. Res.*, 115, D13302, doi:10.1029/2009JD013291, 2010.

491 Clerbaux, C., Boynard, A., Clarisse, L., George, M., Hadji-Lazaro, J., Herbin, H., Hurtmans, D., Pommier,
492 M., Razavi, A., Turquety, S., Wespes, C. and Coheur, P.-F.: Monitoring of atmospheric composition using
493 the thermal infrared IASI/MetOp sounder, *Atmos. Chem. Phys.*, 9(16), 6041–6054, doi:10.5194/acp-9-
494 6041-2009, 2009.

495 Crevoisier, C., Clerbaux, C., Guidard, V., Phulpin, T., Armante, R., Barret, B., Camy-Peyret, C.,
496 Chaboureaud, J.-P., Coheur, P.-F., Cr peau, L., Dufour, G., Labonnote, L., Lavanant, L., Hadji-Lazaro, J.,
497 Herbin, H., Jacquinet-Husson, N., Payan, S., P quignot, E., Pierangelo, C., Sellitto, P., and Stubenrauch,
498 C.: Towards IASI-New Generation (IASI-NG): impact of improved spectral resolution and radiometric
499 noise on the retrieval of thermodynamic, chemistry and climate variables, *Atmos. Meas. Tech.*, 7,
500 4367–4385, <https://doi.org/10.5194/amt-7-4367-2014>, 2014.

Day, M. C., Zhang, M. and Pandis, S. N.: Evaluation of the ability of the EC tracer method to estimate secondary organic carbon, *Atmos. Environ.*, **112**, 317–325, doi:<https://doi.org/10.1016/j.atmosenv.2015.04.044>, 2015.

Fountoukis, C. and Nenes, A.: ISORROPIA II: a computationally efficient thermodynamic equilibrium model for $K^+Ca^{2+}Mg^{2+}NH_4^+Na^+SO_4^{2-}NO_3^-Cl^-H_2O$ aerosols, *Atmos. Chem. Phys.*, **7**, 4639–4659, <https://doi.org/10.5194/acp-7-4639-2007>, 2007.

Guo, X., Wang, R., Pan, D., Zondlo, M. A., Clarisse, L., Van Damme, M., Whitburn, S., Coheur, P.-F., Clerbaux, C., Franco, B., Golston, L. M., Wendt, L., Sun, K., Tao, L., Miller, D., Mikoviny, T., Müller, M., Wisthaler, A., Tevlin, A. G., Murphy, J. G., Nowak, J. B., Roscioli, J. R., Volkamer, R., Kille, N., Neuman, J. A., Eilerman, S. J., Crawford, J. H., Yacovitch, T. I., Barrick, J. D. and Scarino, A. J.: Validation of IASI Satellite Ammonia Observations at the Pixel Scale Using In Situ Vertical Profiles, *J. Geophys. Res. Atmos.*, **126**(9), e2020JD033475, doi:<https://doi.org/10.1029/2020JD033475>, 2021.

Herrera, B., Bezanilla, A., Blumenstock, T., Dammers, E., Hase, F., Clarisse, L., Magaldi, A., Rivera, C., Stremme, W., Strong, K., Viatte, C., Van Damme, M., and Grutter, M.: Measurement report: Evolution and distribution of NH_3 over Mexico City from ground-based and satellite infrared spectroscopic measurements, *Atmos. Chem. Phys. Discuss.* [preprint], <https://doi.org/10.5194/acp-2022-217>, in review, 2022.

Hersbach, H.; Bell, B.; Berrisford, P.; Hirahara, S.; Horányi, A.; Muñoz-Sabater, J.; Nicolas, J.; Peubey, C.; Radu, R.; Schepers, D.; et al. The ERA5 global reanalysis. *Q. J. R. Meteorol. Soc.* **2020**, *146*, 1999–2049, doi:10.1002/qj.3803.

Hoesly, R. M., Smith, S. J., Feng, L., Klimont, Z., Janssens-Maenhout, G., Pitkanen, T., Seibert, J. J., Vu, L., Andres, R. J., Bolt, R. M., Bond, T. C., Dawidowski, L., Kholod, N., Kurokawa, J.-I., Li, M., Liu, L., Lu, Z., Moura, M. C. P., O'Rourke, P. R. and Zhang, Q.: Historical (1750–2014) anthropogenic emissions of reactive gases and aerosols from the Community Emissions Data System (CEDS), *Geosci. Model Dev.*, **11**(1), 369–408, doi:10.5194/gmd-11-369-2018, 2018.

INECC and SEMARNAT 2018 México, Secretaría del Medio Ambiente de la Ciudad de México. Inventario de Emisiones de la Ciudad de México 2016. Dirección General de Gestión de la Calidad del Aire, Dirección de Programas de Calidad del Aire e Inventario de Emisiones. Ciudad de México. Septiembre, 2018 (<http://www.aire.cdmx.gob.mx/descargas/publicaciones/flippingbook/inventario-emisiones-2016/mobile/inventario-emisiones-2016.pdf>, last access May 28 2021).

Jeong, C.-H., Traub, A., Huang, A., Hilker, N., Wang, J. M., Herod, D., Dabek-Zlotorzynska, E., Celo, V. and Evans, G. J.: Long-term analysis of $PM_{2.5}$ from 2004 to 2017 in Toronto: Composition, sources, and oxidative potential, *Environ. Pollut.*, **263**, 114652, doi:<https://doi.org/10.1016/j.envpol.2020.114652>, 2020.

Karydis, V. A., Tsimpidi, A. P., Lei, W., Molina, L. T., and Pandis, S. N.: Formation of semi volatile inorganic aerosols in the Mexico City Metropolitan Area during the MILAGRO campaign, *Atmos. Chem. Phys.*, **11**, 13305–13323, <https://doi.org/10.5194/acp-11-13305-2011>, 2011.

538 Lanza fame, G. M., Srivastava, D., Favez, O., Bandowe, B. A. M., Shahpoury, P., Lammel, G., Bonnaire,
 539 N., Alleman, L. Y., Couvidat, F., Bessagnet, B. and Albinet, A.: One-year measurements of secondary
 540 organic aerosol (SOA) markers in the Paris region (France): Concentrations, gas/particle partitioning
 541 and SOA source apportionment, *Sci. Total Environ.*, 757, 143921,
 542 doi:<https://doi.org/10.1016/j.scitotenv.2020.143921>, 2021.

543 Larios, A. D., Chebana, F., Godbout, S., Brar, S. K., Valera, F., Palacios, J. H., Avalos Ramirez, A., Saldoval-
 544 Salas, F., Larouche, J. P., Medina-Hernández, D. and Potvin, L.: Analysis of atmospheric ammonia
 545 concentration from four sites in Quebec City region over 2010–2013, *Atmos. Pollut. Res.*, 9(3), 476–
 546 482, doi:<https://doi.org/10.1016/j.apr.2017.11.001>, 2018.

547 Lee, P. K. H., Brook, J. R., Dabek-Zlotorzynska, E. and Mabury, S. A.: Identification of the Major Sources
 548 Contributing to PM_{2.5} Observed in Toronto, *Environ. Sci. Technol.*, 37(21), 4831–4840,
 549 doi:10.1021/es026473i, 2003.

550 McDuffie, E. E., Martin, R. V., Spadaro, J. V., Burnett, R., Smith, S. J., O'Rourke, P., Hammer, M. S., van
 551 Donkelaar, A., Bindle, L., Shah, V., Jaeglé, L., Luo, G., Yu, F., Adeniran, J. A., Lin, J. and Brauer, M.: Source
 552 sector and fuel contributions to ambient PM_{2.5} and attributable mortality across multiple spatial
 553 scales, *Nat. Commun.*, 12(1), 3594, doi:10.1038/s41467-021-23853-y, 2021.

554 Molina, L. T., Madronich, S., Gaffney, J. S., Apel, E., de Foy, B., Fast, J., Ferrare, R., Herndon, S., Jimenez,
 555 J. L., Lamb, B., Osornio-Vargas, A. R., Russell, P., Schauer, J. J., Stevens, P. S., Volkamer, R., & Zavala, M.
 556 (2010). An overview of the MILAGRO 2006 Campaign: Mexico City emissions and their transport and
 557 transformation. *Atmospheric Chemistry and Physics*, 10(18), 8697–8760. [https://doi.org/10.5194/acp-](https://doi.org/10.5194/acp-10-8697-2010)
 558 [10-8697-2010](https://doi.org/10.5194/acp-10-8697-2010)

559 Murray, C. J. L., Aravkin, A. Y., Zheng, P., Abbafati, C., Abbas, K. M., Abbasi-Kangevari, M., Abd-Allah,
 560 F., Abdelalim, A., Abdollahi, M., Abdollahpour, I., Abegaz, K. H., Abolhassani, H., Aboyans, V., Abreu, L.
 561 G., Abrigo, M. R. M., Abualhasan, A., Abu-Raddad, L. J., Abushouk, A. I., Adabi, M., Adekanmbi, V.,
 562 Adeoye, A. M., Adetokunboh, O. O., Adham, D., Advani, S. M., Agarwal, G., Aghamir, S. M. K., Agrawal,
 563 A., Ahmad, T., Ahmadi, K., Ahmadi, M., Ahmadi, H., Ahmed, M. B., Akalu, T. Y., Akinyemi, R. O.,
 564 Akinyemiju, T., Akombi, B., Akunna, C. J., Alahdab, F., Al-Aly, Z., Alam, K., Alam, S., Alam, T., Alanezi, F.
 565 M., Alanzi, T. M., Alemu, B., Wassihun, Alhabib, K. F., Ali, M., Ali, S., Alicandro, G., Alinia, C., Alipour, V.,
 566 Alizade, H., Aljunid, S. M., Alla, F., Allebeck, P., Almasi-Hashiani, A., Al-Mekhlafi, H. M., Alonso, J.,
 567 Altirkawi, K. A., Amini-Rarani, M., Amiri, F., Amugsi, D. A., Ancuceanu, R., Anderlini, D., Anderson, J. A.,
 568 Andrei, C. L., Andrei, T., Angus, C., Anjomshoa, M., Ansari, F., Ansari-Moghaddam, A., Antonazzo, I. C.,
 569 Antonio, C. A. T., Antony, C. M., Antriyandarti, E., Anvari, D., Anwer, R., Appiah, S. C. Y., Arabloo, J.,
 570 Arab-Zozani, M., Ariani, F., Armoon, B., Ärnlöv, J., Arzani, A., Asadi-Aliabadi, M., Asadi-Pooya, A. A.,
 571 Ashbaugh, C., Assmus, M., Atafar, Z., Atnafu, D. D., Atout, M. M. W., Ausloos, F., Ausloos, M., Ayala
 572 Quintanilla, B. P., Ayano, G., Ayanore, M. A., Azari, S., Azarian, G., Azene, Z. N., et al.: Global burden of
 573 87 risk factors in 204 countries and territories, 1990–2019: a systematic analysis for the Global
 574 Burden of Disease Study 2019, *Lancet*, 396(10258), 1223–1249, doi:10.1016/S0140-6736(20)30752-2,
 575 2020.

576 NOM-025-SSA1-2021: NORMA Oficial Mexicana NOM-025-SSA1-2021, Salud ambiental. Criterio para
 577 evaluar la calidad del aire ambiente, con respecto a las partículas suspendidas PM₁₀ y PM_{2.5}. Valores

578 normados para la concentración de partículas suspendidas PM₁₀ y PM_{2.5} en el aire ambiente, como
579 medida de protección a la salud de la población, Diario Oficial de la Federación 27 octubre 2021,
580 https://www.dof.gob.mx/nota_detalle.php?codigo=5633855&fecha=27/10/2021#gsc.tab=0, last
581 access August 2022.

582 Nair, A. A. and Yu, F.: Quantification of Atmospheric Ammonia Concentrations: A Review of Its
583 Measurement and Modeling, *Atmosphere* (Basel), 11(10), doi:10.3390/atmos11101092, 2020.

584 Ojeda-Castillo, V., Alonso-Romero, S., Mena, L. H.-, Álvarez-Chávez, P. E. and del Real-Olvera, J.: Air
585 Pollution in an Urban Area of Mexico: Sources of Emission (Vehicular, Natural, Industrial, and Brick
586 Production), in *Air Pollution*, edited by J. D. R. Olvera, IntechOpen, Rijeka., 2019.

587 Pai, S. J., Heald, C. L., Pierce, J. R., Farina, S. C., Marais, E. A., Jimenez, J. L., Campuzano-Jost, P., Nault,
588 B. A., Middlebrook, A. M., Coe, H., Shilling, J. E., Bahreini, R., Dingle, J. H. and Vu, K.: An evaluation of
589 global organic aerosol schemes using airborne observations, *Atmos. Chem. Phys.*, 20(5), 2637–2665,
590 doi:10.5194/acp-20-2637-2020, 2020.

591 Paulot, F. and Jacob, D. J.: Hidden Cost of U.S. Agricultural Exports: Particulate Matter from Ammonia
592 Emissions, *Environ. Sci. Technol.*, 48(2), 903–908, doi:10.1021/es4034793, 2014.

593 Petit, J.-E., Amodeo, T., Meleux, F., Bessagnet, B., Menut, L., Grenier, D., Pellan, Y., Ockler, A., Rocq, B.,
594 Gros, V., Sciare, J. and Favez, O.: Characterising an intense PM pollution episode in March 2015 in
595 France from multi-site approach and near real time data: Climatology, variabilities, geographical origins
596 and model evaluation, *Atmos. Environ.*, 155, 68–84,
597 doi:<https://doi.org/10.1016/j.atmosenv.2017.02.012>, 2017.

598 Petit, J.-E., Favez, O., Sciare, J., Crenn, V., Sarda-Estève, R., Bonnaire, N., Močnik, G., Dupont, J.-C.,
599 Haeffelin, M. and Leoz-Garziandia, E.: Two years of near real-time chemical composition of submicron
600 aerosols in the region of Paris using an Aerosol Chemical Speciation Monitor (ACSM) and a multi-
601 wavelength Aethalometer, *Atmos. Chem. Phys.*, 15(6), 2985–3005, doi:10.5194/acp-15-2985-2015,
602 2015.

603 Potter, P., Ramankutty, N., Bennett, E. M., & Donner, S. D. (2010). Characterizing the Spatial Patterns
604 of Global Fertilizer Application and Manure Production. *Earth Interactions*, 14(2), 1–22.
605 <https://doi.org/10.1175/2009EI288.1>

606 RANDERSON, J. T., VAN DER WERF, G. R., GIGLIO, L., COLLATZ, G. J. and KASIBHATLA, P. S.: Global Fire
607 Emissions Database, Version 4.1 (GFEDv4), , doi:10.3334/ORNLDAAAC/1293, 2017.

608 Retama, A., Ramos-Cerón, M., Rivera-Hernández, O., Allen, G. and Velasco, E.: Aerosol optical
609 properties and brown carbon in Mexico City, *Environ. Sci. Atmos.*, 2(3), 315–334,
610 doi:10.1039/D2EA00006G, 2022.

611 Retama, A., Neria-Hernández, A., Jaimes-Palomera, M., Rivera-Hernández, O., Sánchez-Rodríguez, M.,
612 López-Medina, A. and Velasco, E.: Fireworks: A major source of inorganic and organic aerosols during
613 Christmas and New Year in Mexico City, *Atmos. Environ.* X, 2, 100013,
614 doi:<https://doi.org/10.1016/j.aeaoa.2019.100013>, 2019.

615 REYNOLDS, C. M. and WOLF, D. C.: EFFECT OF SOIL MOISTURE AND AIR RELATIVE HUMIDITY ON
 616 AMMONIA VOLATILIZATION FROM SURFACE-APPLIED UREA, *Soil Sci.*, 143(2) [online] Available from:
 617 [https://journals.lww.com/soilsci/Fulltext/1987/02000/EFFECT_OF_SOIL_MOISTURE_AND_AIR_RELAT](https://journals.lww.com/soilsci/Fulltext/1987/02000/EFFECT_OF_SOIL_MOISTURE_AND_AIR_RELATIVE_HUMIDITY.10.aspx)
 618 [IVE_HUMIDITY.10.aspx](https://journals.lww.com/soilsci/Fulltext/1987/02000/EFFECT_OF_SOIL_MOISTURE_AND_AIR_RELATIVE_HUMIDITY.10.aspx), 1987.

619 Salcedo, D., Alvarez-Ospina, H., Peralta, O., & Castro, T. (2018). PM1 Chemical Characterization during
 620 the ACU15 Campaign, South of Mexico City. *Atmosphere*, 9(6). <https://doi.org/10.3390/atmos9060232>

621 Secretaría del Medio Ambiente de la Ciudad de México. Calidad del aire en la Ciudad de México,
 622 Informe 2018. [Internet]. Dirección General de Calidad del Aire, Dirección de Monitoreo de Calidad del
 623 Aire: Ciudad de México; 2020. Available from:
 624 <http://www.aire.cdmx.gob.mx/default.php?opc=Z6BhnmI>.

625 Sciare, J., d'Argouges, O., Zhang, Q. J., Sarda-Estève, R., Gaimoz, C., Gros, V., Beekmann, M. and
 626 Sanchez, O.: Comparison between simulated and observed chemical composition of fine aerosols in
 627 Paris (France) during springtime: contribution of regional versus continental emissions, *Atmos. Chem.*
 628 *Phys.*, 10(24), 11987–12004, doi:10.5194/acp-10-11987-2010, 2010.

629 Stein, A. F., Draxler, R. R., Rolph, G. D., Stunder, B. J. B., Cohen, M. D. and Ngan, F.: NOAA's HYSPLIT
 630 Atmospheric Transport and Dispersion Modeling System, *Bull. Am. Meteorol. Soc.*, 96(12), 2059–2077,
 631 doi:10.1175/BAMS-D-14-00110.1, 2015.

632 Sutton, M. A., Reis, S., Riddick, S. N., Dragosits, U., Nemitz, E., Theobald, M. R., Tang, Y. S., Braban, C.
 633 F., Vieno, M., Dore, A. J., Mitchell, R. F., Wanless, S., Daunt, F., Fowler, D., Blackall, T. D., Milford, C.,
 634 Flechard, C. R., Loubet, B., Massad, R., Cellier, P., Personne, E., Coheur, P. F., Clarisse, L., Van Damme,
 635 M., Ngadi, Y., Clerbaux, C., Skjøth, C. A., Geels, C., Hertel, O., Wichink Kruit, R. J., Pinder, R. W., Bash, J.
 636 O., Walker, J. T., Simpson, D., Horváth, L., Misselbrook, T. H., Bleeker, A., Dentener, F. and de Vries, W.:
 637 Towards a climate-dependent paradigm of ammonia emission and deposition, *Philos. Trans. R. Soc.*
 638 *Lond. B. Biol. Sci.*, 368(1621), 20130166, doi:10.1098/rstb.2013.0166, 2013.

639 von Bobruzki, K., Braban, C. F., Famulari, D., Jones, S. K., Blackall, T., Smith, T. E. L., Blom, M., Coe, H.,
 640 Gallagher, M., Ghalaieny, M., McGillen, M. R., Percival, C. J., Whitehead, J. D., Ellis, R., Murphy, J.,
 641 Mohacsi, A., Pogany, A., Junninen, H., Rantanen, S., Sutton, M. A. and Nemitz, E.: Field inter-
 642 comparison of eleven atmospheric ammonia measurement techniques, *Atmos. Meas. Tech.*, 3(1), 91–
 643 112, doi:10.5194/amt-3-91-2010, 2010.

644 Van der Gon, H. A. C., Bergström, R., Fountoukis, C., Johansson, C., Pandis, S. N., Simpson, D. and
 645 Visschedijk, A. J. H.: Particulate emissions from residential wood combustion in Europe – revised
 646 estimates and an evaluation, *Atmos. Chem. Phys.*, 15(11), 6503–6519, doi:10.5194/acp-15-6503-2015,
 647 2015.

648 Van Damme, M., Clarisse, L., Franco, B., Sutton, M. A., Erisman, J. W., Wichink Kruit, R., van Zanten,
 649 M., Whitburn, S., Hadji-Lazaro, J., Hurtmans, D., Clerbaux, C., & Coheur, P.-F.: Global, regional and
 650 national trends of atmospheric ammonia derived from a decadal (2008–2018) satellite record.
 651 *Environmental Research Letters*, 16(5), 55017. <https://doi.org/10.1088/1748-9326/abd5e0>, 2021.

652 Van Damme, M., Clarisse, L., Whitburn, S., Hadji-Lazaro, J., Hurtmans, D., Clerbaux, C. and Coheur, P.-
653 F.: Industrial and agricultural ammonia point sources exposed, *Nature*, 564(7734), 99–103,
654 doi:10.1038/s41586-018-0747-1, 2018.

655 Van Damme, M., Whitburn, S., Clarisse, L., Clerbaux, C., Hurtmans, D., and Coheur, P.-F.: Version 2 of
656 the IASI NH₃ neural network retrieval algorithm: near-real-time and reanalysed datasets, *Atmos. Meas.*
657 *Tech.*, 10, 4905–4914, <https://doi.org/10.5194/amt-10-4905-2017>, 2017.

658 Vega, E., Eidels, S., Ruiz, H., López-Veneroni, D., Sosa, G., Gonzalez, E., Watson, J. G., Edgerton, S. A.,
659 Gasca, J., Mora, V., Reyes, E., Sánchez-Reyna, G., Villaseñor, R. and Chow, J. C.: Particulate Air Pollution
660 in Mexico City: A Detailed View, *Aerosol Air Qual. Res.*, 10(3), 193–211,
661 doi:10.4209/aaqr.2009.06.0042, 2010.

662 Viatte, C., Petit, J.-E., Yamanouchi, S., Van Damme, M., Doucerain, C., Germain-Piaulenne, E., Gros, V.,
663 Favez, O., Clarisse, L., Coheur, P.-F., Strong, K. and Clerbaux, C.: Ammonia and PM_{2.5} air pollution in
664 paris during the 2020 covid lockdown, *Atmosphere (Basel)*, 12(2), doi:10.3390/atmos12020160, 2021.

665 Viatte, C., Wang, T., Van Damme, M., Dammers, E., Meleux, F., Clarisse, L., Shephard, M. W., Whitburn,
666 S., François Coheur, P., Cady-Pereira, K. E. and Clerbaux, C.: Atmospheric ammonia variability and link
667 with particulate matter formation: A case study over the Paris area, *Atmos. Chem. Phys.*, 20(1),
668 doi:10.5194/acp-20-577-2020, 2020.

669 Wang, Q., Jacob, D. J., Spackman, J. R., Perring, A. E., Schwarz, J. P., Moteki, N., Marais, E. A., Ge, C.,
670 Wang, J. and Barrett, S. R. H.: Global budget and radiative forcing of black carbon aerosol: Constraints
671 from pole-to-pole (HIPPO) observations across the Pacific, *J. Geophys. Res. Atmos.*, 119(1), 195–206,
672 doi:<https://doi.org/10.1002/2013JD020824>, 2014.

673 Yamanouchi, S., Viatte, C., Strong, K., Lutsch, E., Jones, D. B. A., Clerbaux, C., Van Damme, M., Clarisse,
674 L., and Coheur, P.-F.: Multiscale observations of NH₃ around Toronto, Canada, *Atmos. Meas. Tech.*, 14,
675 905–921, <https://doi.org/10.5194/amt-14-905-2021>, 2021.

676 Yao, X. and Zhang, L.: Causes of Large Increases in Atmospheric Ammonia in the Last Decade across
677 North America, *ACS omega*, 4(26), 22133–22142, doi:10.1021/acsomega.9b03284, 2019.

678 Zellweger, C., Hüglin, C., Klausen, J., Steinbacher, M., Vollmer, M., and Buchmann, B.: Inter-comparison
679 of four different carbon monoxide measurement techniques and evaluation of the long-term carbon
680 monoxide time series of Jungfraujoch, *Atmos. Chem. Phys.*, 9, 3491–3503,
681 <https://doi.org/10.5194/acp-9-3491-2009>, 2009.

682

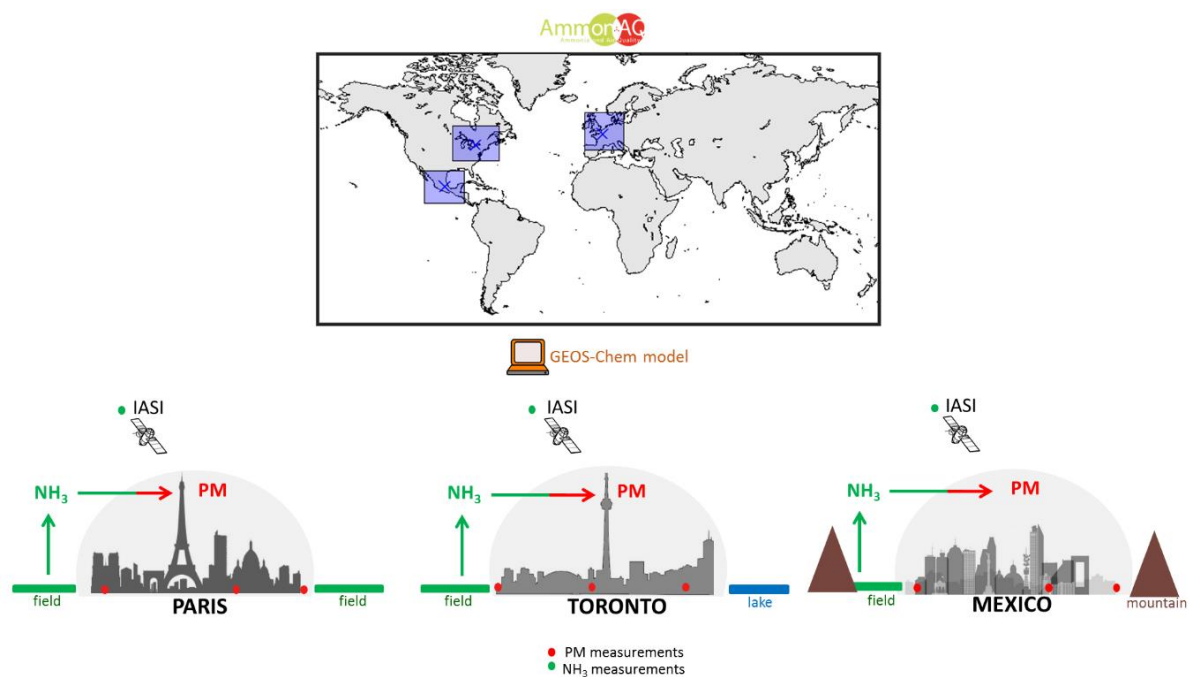


Figure 1: schematic representation of the AmmonAQ project. Upper panel: the three study regions investigated (in blue rectangles). Lower panel: presentation of each city and regional domain and different datasets used.

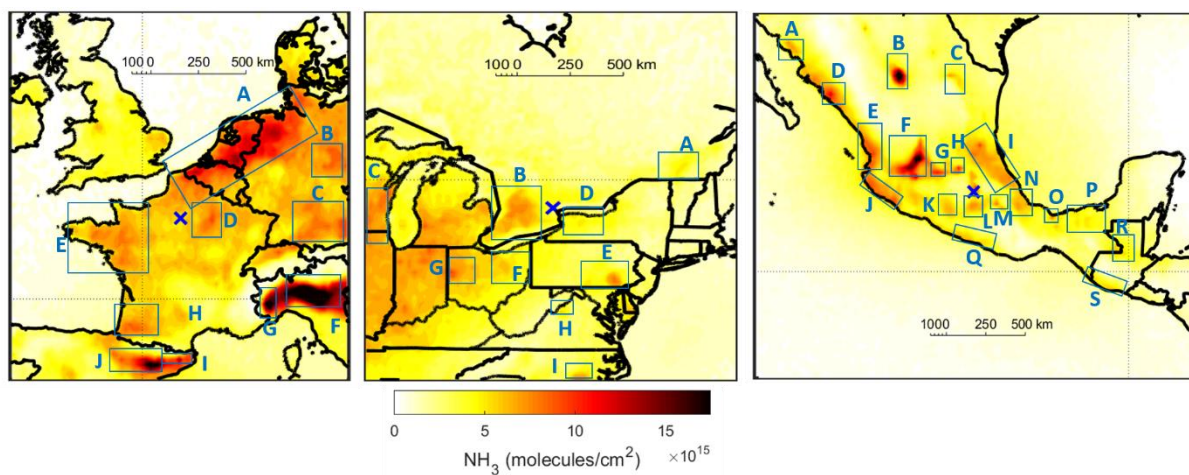


Figure 2: Source region identification of NH_3 derived from 10 years average of IASI total columns (molecules/ cm^2) from 2008 to 2017. The blue crosses indicate Paris, Toronto, and Mexico cities locations.

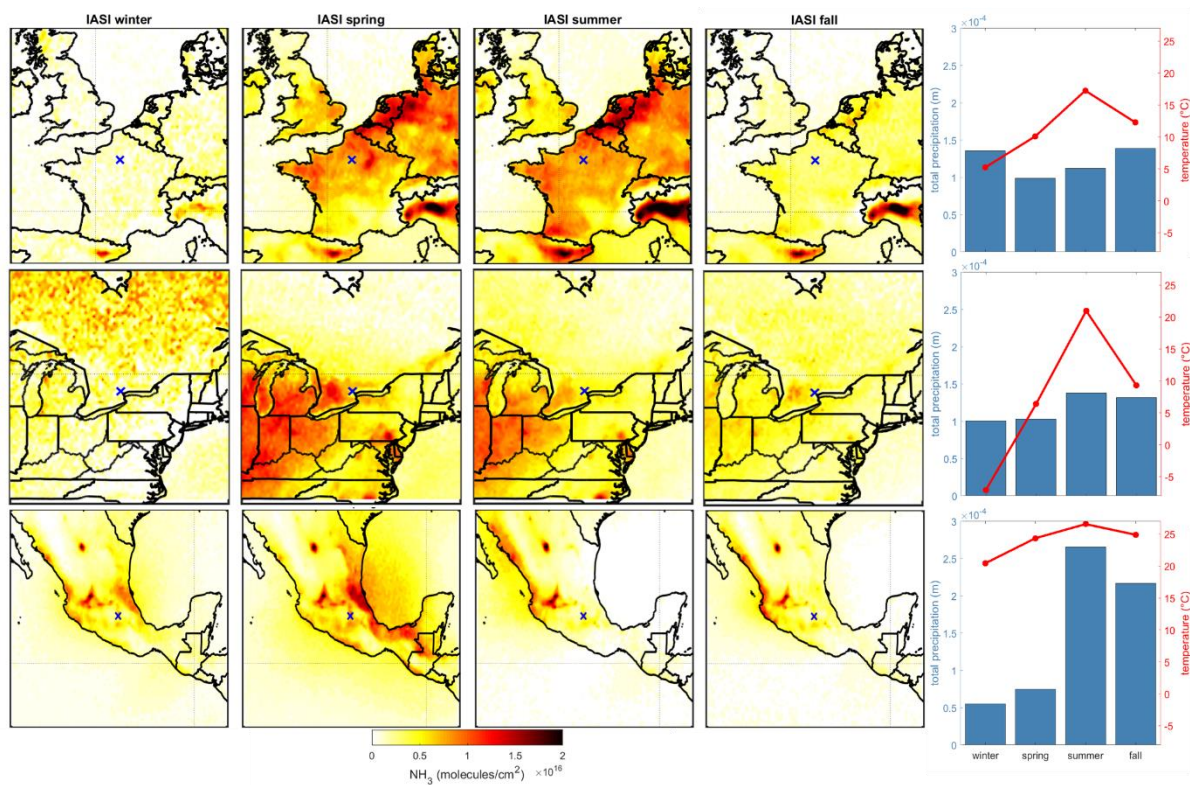


Figure 3: Seasonal maps of NH_3 total columns (molecules/ cm^2) derived from 10 years (2008-2017) of IASI observations, along with seasonal means of atmospheric temperature (red line) and precipitation (blue bar chart) over the Europe (upper panels), North America (middle panels), and southern North America (lower panels) regions.

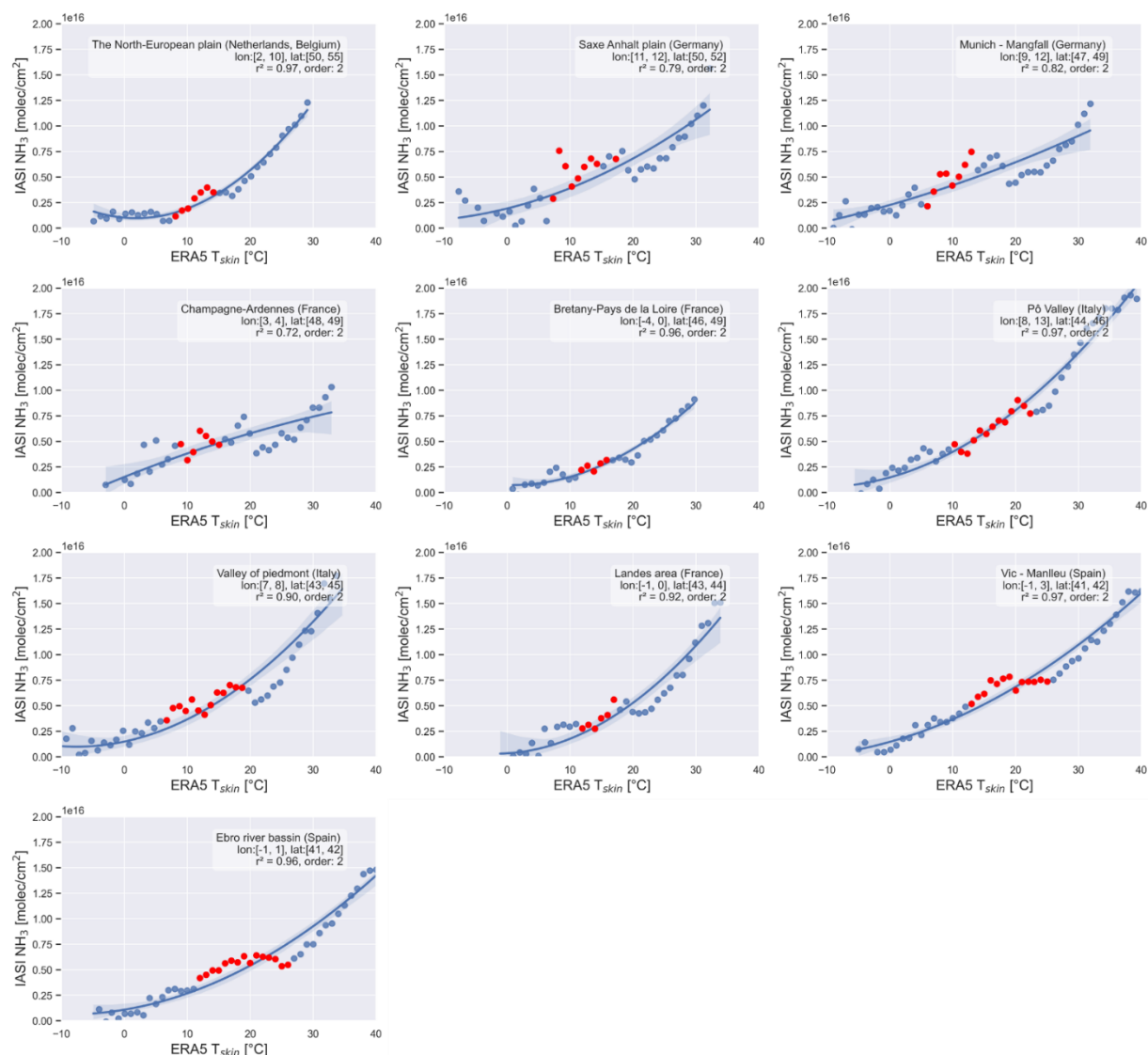


Figure 4: Yearly IASI NH_3 total columns ($\text{molecules}/\text{cm}^2$) averaged per bins of ERA5 skin temperatures ($^{\circ}\text{C}$), with an interval of 1°C between each consecutive bin. The red circles denote the growing seasons, at least 60% of the NH_3 is detected during March-May and Sept-Nov periods. See Figure 2 and Table 1 for the localization of the sub-regions around Europe.

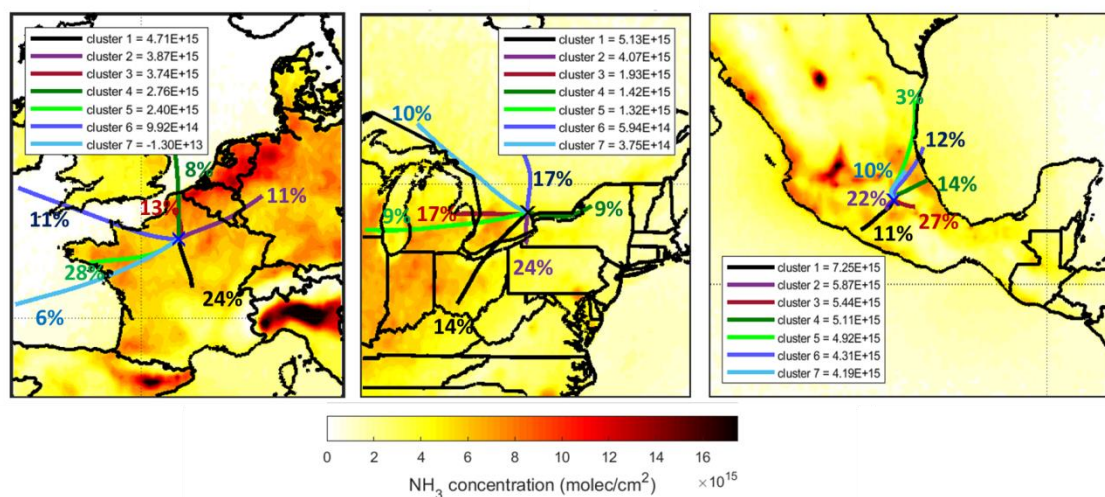


Figure 5: Seven cluster-mean backward trajectories over the Europe, North America, and southern North America regions for the whole time period between 2008 and 2017. Back-trajectories are color-coded in function of the corresponding NH_3 concentrations measured inside the cities. The numbers indicate the percentage of trajectories allocated to a cluster.

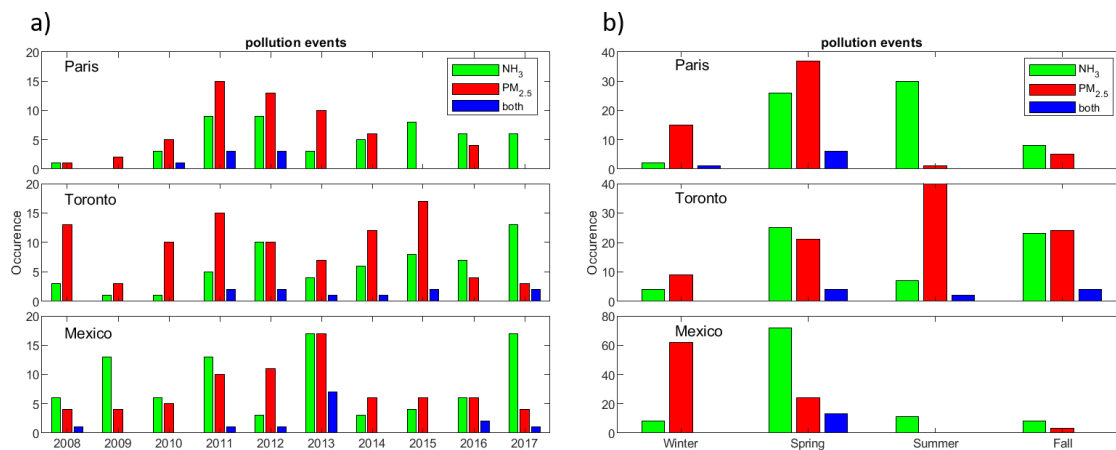


Figure 6: Annual (a) and seasonal (b) occurrence of pollution events of NH_3 (green bars), $\text{PM}_{2.5}$ (red bars), and NH_3 and $\text{PM}_{2.5}$ simultaneous (blue bars) detected from 2008 to 2017 in Paris (upper panel), Toronto (middle panel), and Mexico (lower panel) cities.

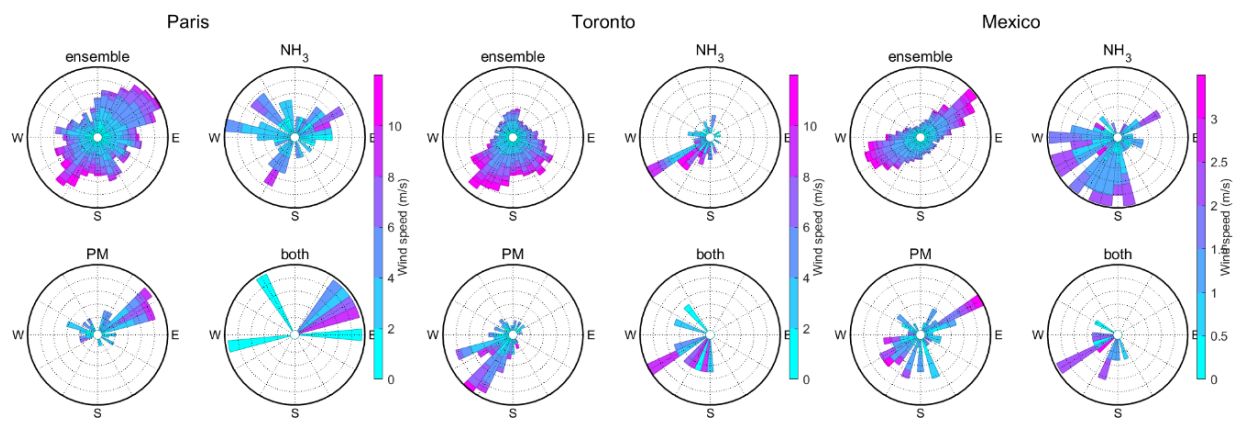


Figure 7: Wind roses corresponding to the ensemble of all observations, the NH_3 , $\text{PM}_{2.5}$, and both NH_3 and $\text{PM}_{2.5}$ simultaneous pollution events derived from 2008 to 2017 over Paris (left panels), Toronto (middle panels), and Mexico (right panels) cities.

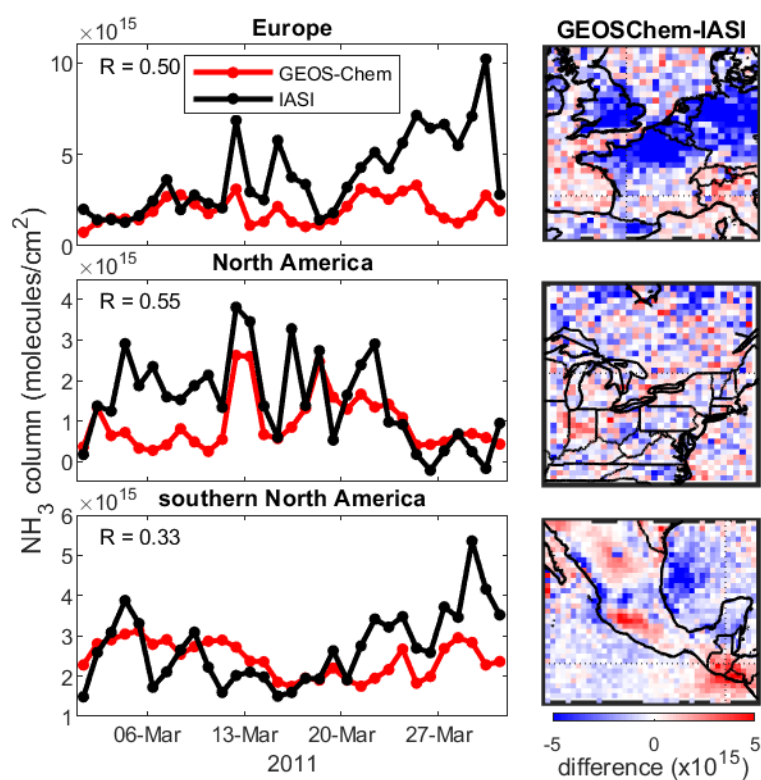


Figure 8: Left: time-series of daily NH_3 columns derived from IASI (black lines) and the GEOS-Chem model (red lines) over Europe (upper panel), North America (middle panel), and southern North America (lower panel). Right: maps of NH_3 columns (in molecules/cm²) differences between IASI and GEOS-Chem model (model-observations) for March 2011.

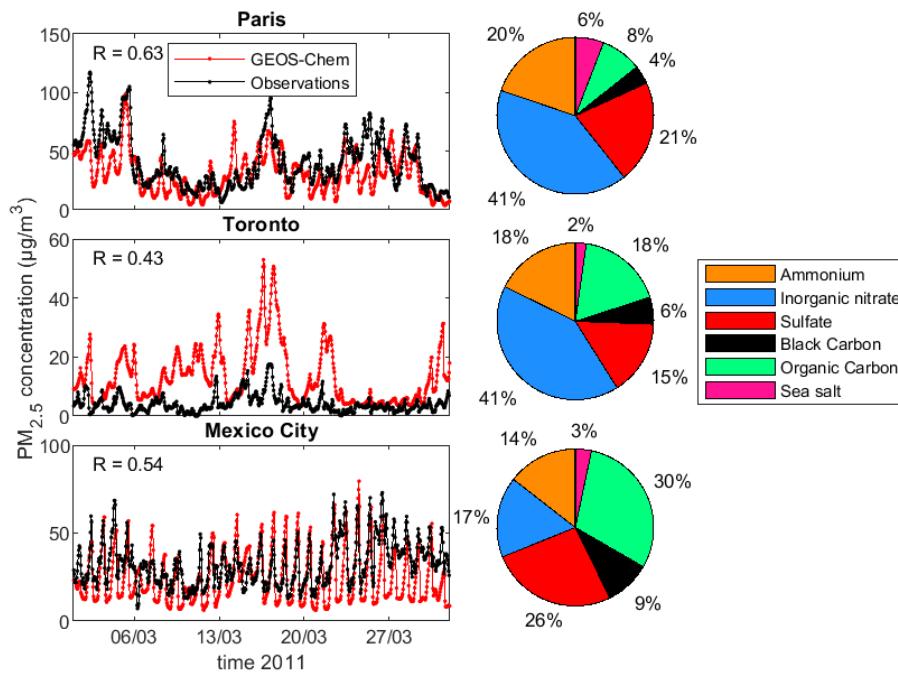


Figure 9: left: Time-series of hourly PM_{2.5} ($\mu\text{g}/\text{m}^3$) derived from surface observations (black lines) and the GEOS-Chem model (red lines) over Paris (upper panel), Toronto (middle panel), and Mexico (lower panel) cities for March 2011. Right: PM_{2.5} speciation (% in total mass) derived from the GEOS-Chem run for March 2011.

729 Table 1: List of NH₃ source regions identified using 10-years average of IASI total columns (molecules/cm²) over
730 the Europe, North America, and southern North America regions.

Europe [41°-59°N ; -11.25°- 16.25°E]		North America [35°-53°N ; 93.75°-63.75°W]		Southern North America [9°-29°N ; 113.75°-86.25°W]	
A	The North-European plain ^{1,2}	A	Granby (Canada)	A	Obregon (Mexico) ¹
B	Saxe Anhalt plain (Germany)	B	Elmira-Kitchener-Guelph (Canada)	B	Torreon (Mexico) ^{1,2}
C	Munich - Mangfall (Germany)	C	Brillion area (U.S.A.)	C	Garcia (Mexico)** ¹
D	Champagne-Ardenne (France)	D	New-York state (U.S.A.)	D	Culiacancito (Mexico) ^{1,2}
E	Bretany-Pays de la Loire (France) ²	E	Lancaster county (U.S.A.)	E	Nayarit (Mexico)
F	Pô Valley (Italy) ^{1,2}	F	Wayne county (U.S.A.)	F	Jalostotitlan-San Juan de Los Lagos (Mexico) ^{1,2}
G	Valley of piedmont (Italy) ^{1,2}	G	Celina-Coldwater (U.S.A.) ¹	G	Salamanca – Villagran (Mexico)* ¹
H	Landes area (France)	H	Shenandoah Valley-Bridgewater (U.S.A.) ¹	H	Ezequiel Montes (Mexico) ^{1,2}
I	Vic - Manlleu (Spain) ^{1,2}	I	Lenoir County (U.S.A.)	I	Tampaon, Loma Alta (Mexico) ¹
J	Ebro river bassin (Spain) ^{1,2}			J	Tecoman (Mexico)
				K	Coyuca de Catalan (Mexico)
				L	Morelos (Mexico)
				M	Tochtepec-Tehuacan (Mexico) ¹
				N	South of Veracruz (Mexico)
				O	Cosolaecaque (Mexico)* ¹
				P	Tabasco (Mexico)
				Q	Guerrero (Mexico)
				R	Chisec (Guatemala)
				S	Texcuaco (Guatemala)

*Fertilizer industry ** Soda ash industry

¹ Van Damme et al., 2018; Clarisse et al., 2019

² Dammers et al., 2019

731